

Relic jet activity in “Hanny’s Voorwerp” revealed by the LOFAR Two metre Sky Survey

D. J. B. Smith,^{*} M. G. Krause, M. J. Hardcastle and A. B. Drake

Centre for Astrophysics Research, Department of Physics, Astronomy and Mathematics, University of Hertfordshire, Hatfield AL10 9AB, UK

Accepted XXX. Received YYY; in original form ZZZ

ABSTRACT

We report new observations of “Hanny’s Voorwerp” (hereafter HV) taken from the second data release of the LOFAR Two-metre Sky Survey (LoTSS). HV is a highly-ionised region in the environs of the galaxy IC2497, first discovered by the Galaxy Zoo project. The new 150 MHz observations are considered in the context of existing multi-frequency radio data and archival narrow-band imaging from the *Hubble Space Telescope*, centred on the [OIII] emission line. The combined sensitivity and spatial resolution of the LoTSS data – which far exceed what was previously available at radio frequencies – reveal clear evidence for large-scale extended emission emanating from the nucleus of IC2497. The radio jet appears to have punched a hole in the neutral gas halo, in a region co-located with HV. The new 150 MHz data, alongside newly-processed archival 1.64 GHz eVLA data, reveal that the extended emission has a steep spectrum, implying an age $> 10^8$ yr. The jet supplying the extended 150 MHz structure must have “turned off” long before the change in X-ray luminosity reported in recent works. In this picture, a combination of jet activity and the influence of the radiatively efficient active galactic nucleus are responsible for the unusual appearance of HV.

Key words: Galaxies: active – Galaxies: jets – Galaxies: peculiar

1 INTRODUCTION

Hanny’s Voorwerp (hereafter HV) is a region of highly ionised material tens of kpc in projected size, which is located near the $z = 0.05$ galaxy IC2497. HV was originally reported in [Lintott et al. \(2009\)](#), having been discovered during visual classification of galaxies in the Sloan Digital Sky Survey (SDSS; [York et al. 2000](#)), as part of the Galaxy Zoo project ([Lintott et al. 2008](#)). HV was identified as a result of its unusual morphology and extremely bright [OIII] emission falling in the SDSS g' band filter. [Lintott et al. \(2009\)](#) suggested that HV could be explained either as a highly photoionised region resulting from an active galactic nucleus (AGN) with an unusual dust geometry that prevents it from ionising the host galaxy’s own nuclear gas, or as a “light echo” resulting from a dramatic change in the luminosity of the central source over the past 10^5 years.

As well as discovering a halo containing $\sim 10^9 M_{\odot}$ of HI gas surrounding IC2497 and HV, [Józsa et al. \(2009, hereafter J09\)](#) provided the first evidence of jets visible as a marginal extension to an already elliptical restoring beam in both 1.4 and 4.9 GHz observations in the direction of HV. This extension is not visible in 1.4 GHz observations from the Faint Images of the Radio Sky at Twenty-centimetres survey (FIRST; [Becker et al. 1995](#)), the NRAO VLA Sky Survey (NVSS; [Condon et al. 1998](#)), the Westerbork Northern Sky Survey (WENSS; [Rengelink et al. 1997](#)), or in 150 MHz observations from the TIFR GMRT Sky Survey Alternative Data Release (TGSS-ADR; [Intema et al. 2017](#)). Nevertheless, [Rampadarath et al. \(2010\)](#) further underlined the presence of jets using MERLIN observations to detect two components separated by ~ 300 pc with brightness temperatures in excess of 10^5 K (an upper limit to the brightness temperature that can

be attributed to star forming regions; [Condon et al. 1991](#); [Biggs et al. 2010](#)), though with a significant flux deficit relative to the integrated measurements reported by J09 indicating the presence of a resolved nuclear starburst in IC2497.

Hubble Space Telescope observations in both broad- and narrow-band filters centred on the [OIII] and $H\alpha$ + [NIII] emission lines ([Keel et al. 2012a](#)) found evidence for large regions photoionised by AGN activity, with evidence for some sites within HV dominated by star formation. [Keel et al. \(2012a\)](#) also hypothesised about the role of a previous major merger in stirring up the H I gas around IC2497, and producing the bar and strong warping visible in the disk of IC2497.

Several works have looked at HV at X-ray wavelengths, including [Schawinski et al. \(2010\)](#) and [Sartori et al. \(2018\)](#). These works show that HV contains a Compton-thick AGN which has recently (in the last $\sim 70,000$ yr) undergone a dramatic change in luminosity, similar to the change suggested by [Keel et al. \(2012b\)](#) and [Lintott et al. \(2009\)](#). Most recently, [Fabbiano & Elvis \(2019\)](#) found evidence for extended soft X-ray emission in *Chandra* data of HV, spatially consistent (albeit at low-resolution and with low statistical significance) with the direction of the extension similar to that in the radio data observed by J09.

Our observational capabilities at radio frequencies have exploded since HV was first studied with interferometry by J09 and [Rampadarath et al. \(2010\)](#). The capabilities of the Low Frequency Array (LOFAR; [van Haarlem et al. 2013](#)) exemplify the huge steps in survey speed, sensitivity, resolution and imaging capabilities. One of the key drivers for LOFAR since its inception has been to conduct surveys of the whole northern sky, and the LOFAR Two-metre Sky Survey (LoTSS [Shimwell et al. 2017](#)) is well on the way to fulfilling that aim. The first data release (LoTSS DR1; [Duncan et al. 2019](#); [Shimwell et al. 2019](#); [Williams et al. 2019](#)) covered 424 deg^2 over

^{*} E-mail: d.j.b.smith@herts.ac.uk

the HETDEX (Hill et al. 2008) spring field using the LOFAR High Band Antenna (HBA) at a central frequency of 150 MHz with a mean RMS sensitivity $< 100 \mu\text{Jy}$ and resolution around 6 arcsec. As well as the advantages of a huge increase in sensitivity relative to FIRST, LoTSS HBA data benefit from including short and long-baseline observations in the pipeline-processed data products, meaning that it is uniquely sensitive to low-frequency emission on both compact and extended scales. LoTSS also includes even deeper observations over tens of deg^2 in the prime Northern fields with the best ancillary data (Boötes, Lockman Hole and ELAIS-N1) in the first data release of the LoTSS Deep fields (Tasse et al. 2021; Sabater et al. 2021; Kondapally et al. 2021; Duncan et al. 2021).

Progress continues to be rapid; as well as observations at even lower frequencies (using the Low Band Antenna; de Gasperin et al. 2021) and using international baselines to obtain sub-arcsecond resolution (Morabito et al. 2022), the second data release of LoTSS (DR2; Shimwell et al. 2022) reaches a median 150 MHz sensitivity of $84 \mu\text{Jy beam}^{-1}$ over 5700 deg^2 , detects more than 4.3 million 150 MHz sources, and benefits from a range of further improvements to the data processing relative to LoTSS DR1.

In addition to the sensitivity of the LoTSS maps, together with higher frequency data, 150 MHz observations are particularly useful for determining the properties of extragalactic radio sources. Energy loss in a population of relativistic electrons is expected to vary as a function of ν^2 , such that higher frequencies fade more rapidly as the electron population ages, and as a result the degree of radio spectral curvature increases with time. When studied in the context provided by GHz data therefore, low frequency observations can ‘anchor’ the spectrum, and in doing so enable the best measurements of spectral curvature (and therefore the age of the electron population; e.g. Kardashev 1962; Laing & Peacock 1980; Harwood et al. 2013). Using data spanning $325 \text{ MHz} < \nu < 4.9 \text{ GHz}$, J09 reported a flat radio spectrum of the core of IC2497, consistent with a power law such that $S_\nu \propto \nu^{-\alpha}$ with an index of $\alpha = 0.55$, and no evidence for spectral curvature indicating that the core radio source is young.

The IC2497-HV system is thought to be virtually unique in the local Universe (Keel et al. 2012b, 2015). Even in the absence of HV, the unambiguous presence of jets in IC2497 alone would make the system remarkable since Singh et al. (2015) identified only four instances of double radio jets among 187,000 spiral galaxies identified in SDSS imaging (see also Mao et al. 2015; Nesvadba et al. 2021). HV therefore represents a prototype for studying a broad range of phenomena: the variability thought to be inherent in AGN physics, the role of mergers and/or interactions in triggering AGN activity, as well as the influence of AGN activity on the surrounding gas. These are some of the key physical processes required to explain the observed properties of galaxies (see e.g. Silk & Rees 1998; Croton et al. 2006; Alexander & Hickox 2012). In this paper, we examine the properties of IC2497 and HV in the new 150 MHz data from LoTSS DR2, and in newly processed archival 1.6 GHz eVLA data. In Section 2 we describe the data we use, while in Section 3 we present our results before making some concluding remarks in Section 4.

2 DATA

New LoTSS DR2 observations of HV are available from the LOFAR surveys website¹. The properties of the LoTSS DR2 mosaics are described in detail in Shimwell et al. (2022), however the vital

statistics can be summarised as follows. The 150 MHz images are automatically reduced using the latest version of the LoTSS processing pipeline, which uses direction-dependent methods to account for varying ionospheric conditions, giving high quality data with 6-arcsec resolution, and sensitivity to emission on both small and large scales due to the range of baselines available to the Dutch LOFAR array. HV falls within the area covered by the P144+35 mosaic; however, to obtain an optimal image of the region surrounding HV, we produced a self-calibrated image following the method of van Weeren et al. (2021). The resulting image, shown in the left panel of Figure 1, is at the natural resolution of the LOFAR observations using robustness 0.5, and has an elliptical restoring beam with major and minor axes 8.5 and 4.8 arcsec, 1.5 arcsec pixels and a uniform RMS noise level of $92 \mu\text{Jy beam}^{-1}$ across the image. The absolute flux scale of the LoTSS data is thought to be correct at the level of 6 percent.

We obtained archival eVLA data of the region surrounding HV, taken in 2011 in B-configuration (giving excellent sensitivity to extended structures out to angular scales of 2 arcmin). The eVLA data have an effective frequency of 1.64 GHz, with 256 MHz of bandwidth, and provide similar spatial resolution (major and minor beam axes of 4.9 and 3.2 arcsec) to the new LoTSS data. The newly-reduced eVLA map is shown in the right-hand panel of figure 1; based on comparing the flux densities of unresolved sources with FIRST, we conclude that the flux scale is correct to ~ 5 percent. We also obtained the 1.4 GHz WSRT image and H α data cube from J09 (G.I.G. Józsa, private communication).

The HV-IC2497 system was observed using *Advanced Camera for Surveys* (ACS) tunable ramp filters on board the *HST* (Keel et al. 2012a), with the central wavelengths set to sample the redshifted [OIII] and H α emission lines, and integration times of 2570 s and 2750 s respectively. The pointing was chosen so that HV and IC2497 fell within the monochromatic field of view ($40 \text{ arcsec} \times 80 \text{ arcsec}$) and no continuum subtraction was attempted since Lintott et al. (2009) showed that it was unnecessary. The final reduced HST data products from Keel et al. (2012a) were provided by the authors (W.C. Keel, private communication).

3 RESULTS

3.1 Morphology and photometry

Figure 2 shows the new LoTSS 150 MHz mosaic as contours overlaid on a colour composite image derived using the *HST* [OIII] and H α narrow-band images from Keel et al. (2012a). It is clear that as well as an unresolved component coincident with the centre of IC2497, the extension identified by J09 is now resolved into clear jet-related emission spatially coincident with HV, and with a flux density of $10.0 \pm 0.1 \text{ mJy}$. The total flux density of the system at 150 MHz in the new LoTSS mosaic is $97.3 \pm 0.2 \text{ mJy}$. This structure is not detected in the eVLA image (or any of the other assembled radio data), implying that its spectrum is steep.

The flux density of the unresolved core of IC2497 (obtained by subtracting S_ν^{Extended} from S_ν^{Total}) is consistent with the measurement from the TGSS-ADR mosaic once the calibration uncertainties are taken into account, and corresponds to a 150 MHz luminosity of $(5.63 \pm 0.01) \times 10^{23} \text{ W Hz}^{-1}$. Assuming a standard relationship from Heckman & Best (2014) and correcting to 150 MHz following Sabater et al. (2019), this enables us to estimate a mechanical power in the jet of $1.5 \times 10^{36} \text{ W}$. Although it compares well with the Lintott et al. (2009) estimate of HV’s [OIII] luminosity ($1.5 \times 10^{35} \text{ W}$),

¹ www.lofar-surveys.org

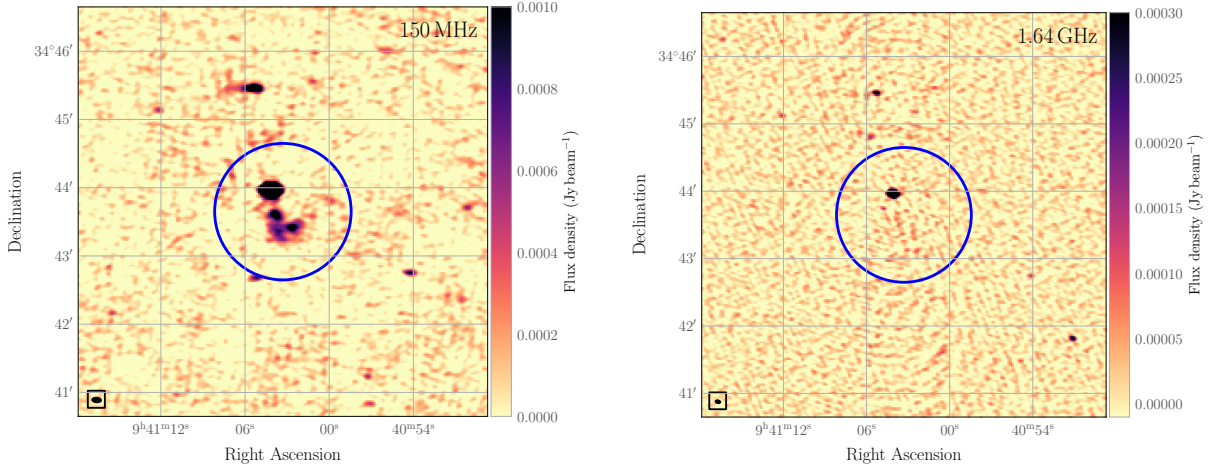


Figure 1. New LoTSS (left) and eVLA (right) images of the region surrounding IC2497 and HV, highlighted with the blue circle, which has a radius of 1 arcmin. The size of the natural-resolution restoring beam is shown as the black ellipse within a box in the lower-left corner of each image. The flux scale is as indicated by the colour bars to the right.

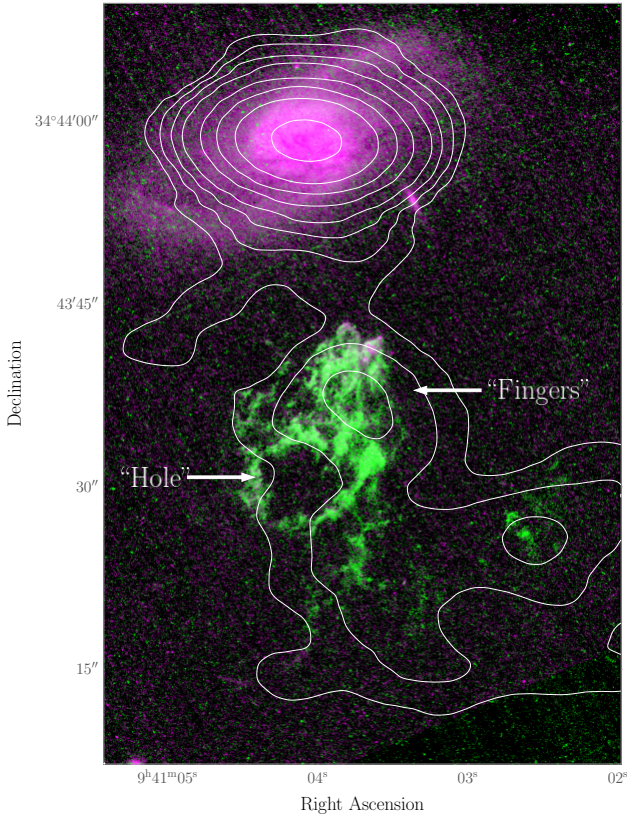


Figure 2. LoTSS 150 MHz map of the region centred on HV (white contours) overlaid on a colour composite built from the [OIII] (green channel) and $H\alpha$ (blue and red channel) narrow-band filter HST images from Keel et al. (2012a). The LoTSS contours, shown in magenta, are at levels of 0.2, 0.5, 1, 2, 5, 10, 20 & 50 mJy beam^{-1} .

the energetics alone preclude the current core activity from making the dominant contribution to the Keel et al. (2012a) estimate of the luminosity required to maintain the ionization of HV ($\sim 10^{38}$ W).

Using the $100 \mu\text{m}$ flux density quoted for IC2497 in the IRAS faint source catalogue (Moshir et al. 1990), we can estimate the star forma-

tion rate (SFR) assuming that the dust is heated solely by young stars, that it has a far-infrared SED similar to M82 (Polletta et al. 2007) and the canonical relationship between far-infrared luminosity and SFR from Kennicutt (1998) adjusted to our adopted initial mass function (IMF) from Chabrier (2003). Doing so, we obtain a far infrared luminosity integrated between $8\text{--}1000 \mu\text{m}$ of $4.1 \times 10^{11} L_{\odot}$ – putting IC2497 in the Luminous Infrared Galaxy (LIRG) class – and an SFR of $\sim 40 M_{\odot} \text{ yr}^{-1}$, although we note that the uncertainties inherent in our choice of SED template and IMF (and therefore the derived SFR) are significant. Nevertheless, comparing the derived SFR with the mass-independent SFR – $L_{150 \text{ MHz}}$ relations from Gürkan et al. (2018) and Smith et al. (2021), reveals no evidence for any radio excess, consistent with the nuclear starburst reported by Rampadarath et al. (2010). Nevertheless, the morphological evidence for the presence of an AGN is conclusive.

To put the new morphological information available from the ~ 6 arcsec resolution LoTSS data in the context of the previously available radio data, in both panels of Figure 3 we overlay the 150 MHz data as magenta contours on a background image showing the H α data from J09. Overlaid in the left panel is the 1.4 GHz WSRT image from J09, shown as blue contours (the WSRT data have an elliptical point spread function of 14×11 arcsec, shown as the blue-filled ellipse in the lower-left corner; Morganti et al. 2004), with the details of the chosen contour levels given in the caption. While at 1.4 GHz the degree of extension in the radio source is perhaps debatable on the basis of visual inspection alone due to the elongated beam along the IC2497–HV direction, this is not true at 150 MHz, where the LoTSS PSF (shown as the magenta ellipse to the lower-left) is more than four times smaller. In the right panel of Figure 3 we show a zoomed version of the central region; for the first time it is clear that the clearly-resolved structure emanating from the nucleus of IC2497 coincides with a minimum in the surrounding $10^9 M_{\odot}$ reservoir of H α gas found by J09 (shown in the background image).

Based on the left panel of Figure 3 it would be tempting to identify the knot of coincident 150 MHz and 1.4 GHz emission on the Northern side of IC2497 as being related to the counter-jet, emanating in the direction opposite to HV. However, inspection of the SDSS images shows that this knot of emission is instead associated with an edge-on late-type galaxy interloper.

Frequency	S_{ν}^{Total} (mJy)	$S_{\nu}^{\text{Extended}}$ (mJy)	Facility/Survey	Reference
150 MHz	97.3 ± 0.2	10.0 ± 0.1	LoTSS	This work
	66.4 ± 8.3		TGSS-ADR	Intema et al. (2017)
325 MHz	51 ± 4.9	3.2 ± 0.2	WENSS	Rengelink et al. (1997)
	20.9 ± 1.1		WSRT	Józsa et al. (2009)
1.4 GHz	18.5 ± 0.6	0.48 ± 0.29	NVSS	Condon et al. (1998)
	16.8 ± 0.9		FIRST	Becker et al. (1995)
1.64 GHz	14.2 ± 0.5		eVLA	This work
4.9 GHz	11.6 ± 0.6		WSRT	Józsa et al. (2009)

Table 1. A compilation of radio frequency flux densities of IC2497 & HV, including both the total (S_{ν}^{Total}) and extended ($S_{\nu}^{\text{Extended}}$) components where available.

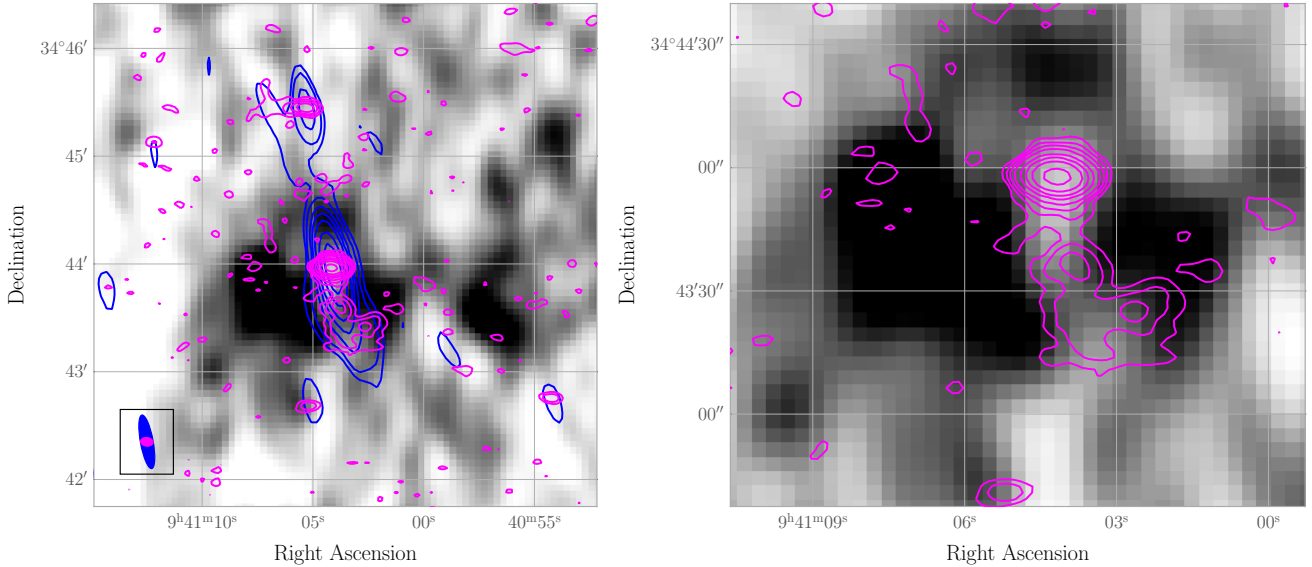


Figure 3. Composite image showing the HI image (background, greyscale) and the new LoTSS data (magenta contours, levels of 0.2, 0.5, 1, 2, 5, 10, 20 & 50 mJy beam^{-1}). In the left panel, the WSRT 1.4 GHz image from [Józsa et al. \(2009\)](#) is shown as blue contours (with contour levels of 0.1, 0.2, 0.5, 1, 2, 5, 10 & 20 mJy beam^{-1}), and the filled ellipses in the box to the bottom left indicate the size of the restoring beam, colour-coded to match the contours. The right panel is zoomed in to highlight the spatial anti-correlation between the jet (magenta contours) and the HI gas (background greyscale) with the same contour levels and colour scale as the left panel.

3.2 Radio spectral index

To examine the radio spectrum of the IC2497-HV system, in Figure 4 we show the total photometry (S_{ν}^{Total}) from Table 1 as filled circles, though we have added calibration uncertainties in quadrature, at the level of 6 percent to the new LoTSS flux density ([Shimwell et al. 2022](#)), and 5 percent to the new eVLA measurements. The photometry is overlaid with a power law with the spectral index $\alpha = 0.55$ found by J09. Despite reaching lower frequencies, the new LoTSS data do not reveal any evidence for spectral curvature in the core; the power law found by J09 continues down to frequencies of 150 MHz at least.

In figure 4, the extended source photometry ($S_{\nu}^{\text{Extended}}$ from Table 1) is shown using square symbols. There are conflicting results for the spectral index of the extended component, depending on whether we use the WSRT or eVLA flux densities, since the nominal 1.64 GHz eVLA flux density of 0.48 ± 0.29 mJy (measured at a spatial resolution similar to the new LoTSS data) is inconsistent with the 1.4 GHz WSRT estimate of 3.2 ± 0.2 mJy. We suggest that the flat spectrum of the extended emission ($\alpha_{150}^{1400} = 0.51 \pm 0.03$) obtained using the WSRT estimated flux density may be an artefact of contamination from the extension in the North-South direction of the WRST point

spread function. Using instead the eVLA flux density alongside the 150 MHz measurement we obtain our best estimate of the extended component's spectral index of $\alpha_{150}^{1640} = 1.25^{+0.28}_{-0.23}$. As the extended structure detected in the LOFAR data is not formally detected in the eVLA image, the spectrum might be even steeper, but we can be confident that $\alpha > 1$.

The steep spectrum implies that the plasma in the extended structure is significantly older than that in the core, as expected if the jet feeding it has ‘turned off’ some time ago. However, since we have measurements at just two frequencies, and a detection only at 150 MHz, detailed analysis is not possible. If we assume that the injection index for this material is $\alpha = 0.55$, estimate a self-consistent equipartition magnetic field strength of around 0.2 nT (based on treating the extended material as a uniformly filled sphere of radius 16 arcsec), and take account of inverse-Compton losses to the CMB at the redshift of HV², then using a Jaffe-Perola model for spectral ageing ([Jaffe & Perola 1973](#)) we find that the spectral age must be

² Calculations were done using the `PSYNCH` Python package <https://github.com/mhardcastle/psynch> which provides an interface to the synchrotron emission code of [Hardcastle et al. \(1998\)](#).

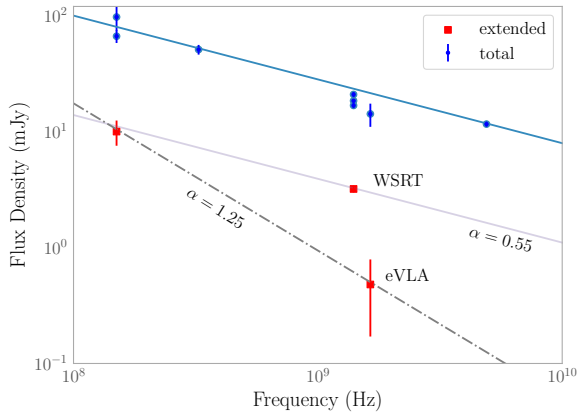


Figure 4. Radio frequency spectra of HV, including values for the total (blue circles) and extended components (red squares), as detailed in Table 1. The solid blue line indicates a power-law spectrum with spectral index $\alpha = -0.55$, while the dotted and dot-dashed lines indicate the spectral index obtained using the 150 MHz data alongside the WSRT 1.4 GHz or eVLA 1.64 GHz flux densities, which are formally inconsistent as discussed in the text.

$> 10^8$ yr to give $\alpha > 1$. Adiabatic expansion of a lobe generated by a now disconnected jet will tend to increase the apparent spectral age, perhaps by an order of magnitude, but this still implies that the jet supplying the extended structure must have turned off long before the change in X-ray luminosity reported by Sartori et al. (2018). Future 60 MHz observations with the LOFAR Low-band Antennae may be able to provide better constraints on the degree of spectral curvature, and therefore on the age of the plasma.

4 DISCUSSION & CONCLUSIONS

We attempt to bring all of this information together as follows. The flat spectral index in the core of IC2497 extends to 150 MHz, and is similar to values for injection indices assumed by jet models (see e.g. Shulevski et al. 2015, for a discussion). This is consistent with the small-scale nuclear jets observed by Rampadarath et al. (2010).

On the other hand, the extended component seen at 150 MHz has a steep spectrum ($\alpha_{150}^{1640} = 1.25^{+0.28}_{-0.23}$), implying an age of order 10^8 yr if the injection index is the same as that measured for the compact component. Other studies based at X-ray wavelengths (e.g. Schwabinski et al. 2010; Sartori et al. 2018) have suggested a timescale of $\sim 10^5$ years for a change in the luminosity of the central engine; however the LoTSS data conclusively show that the jet that generated the extended emission must have been unrelated to that nuclear outburst.

The brightest knots of 150 MHz emission visible in Figure 2 appear co-located with the main star-forming structure at the Northern end of HV, and with the apparently separate (in the *HST* data) component to the West. The Northern 150 MHz knot appears coincident with the filamentary “fingers” located just to the South of the star-forming region located at the Northern tip of HV (which appears pink in figure 2 due to the bright $H\alpha$ emission). These features were first identified in Keel et al. (2012a) as possible evidence of gas entrained by ram pressure of the jet emanating from the core of IC2497. Radiative dissipation in turbulent mixing may contribute to the line emission locally (Krause & Alexander 2007), even though the overall spectrum is dominated by photoionisation (compare below).

The “hole” feature on the South-East side of HV is reminiscent of supernova remnants visible within our own galaxy, although the overall structure and the optical line ratios in this area measured by

Lintott et al. (2009, based on long-slit spectroscopy) and Keel et al. (2012a, based on *HST* narrow-band imaging) are clearly dominated by photoionisation, and therefore not associated with the passage of the jet. Fabbiano & Elvis (2019) reported extended X-ray emission apparent in this area (albeit at low statistical significance) as might also be expected under the hypothesis of a recent explosive event at this location, although no remnant is visible in any of the assembled data.

In the Krause (2005) model, the leading shell of a starburst wind (perhaps resulting from the nuclear starburst suggested to be present in the HV system by Rampadarath et al. 2010) can cool and form a dense, mainly neutral H I shell, if for some reason it encounters enough gas, such as in the post-major merger scenario for IC2497 discussed by Keel et al. (2012a). When a large-scale jet is also present (as is clearly the case based on the new 150 MHz data), it interacts with the shell and pierces a hole in it. In the Krause (2005) simulations, the hole is ~ 20 kpc in diameter, very similar to the radio lobe width observed in HV.

A counterargument to this picture appears to be that in the Lintott et al. (2009) optical spectroscopy, as well as in unpublished integral-field spectroscopy of the HV system using the WIYN-HEXPAK instrument (W.C. Keel, *private communication*) HV has a smooth velocity field showing no evidence of disturbances that might be expected in a jet interaction scenario (see Krause 2005, Fig. 3). While a blue-shifted velocity field that is coherent over many kpc might indeed point to a starburst wind shell, the scenario from Krause (2005) could still describe HV but must be modified. An element of physics that was missing in the latter simulations was the Vishniac shell instability (Vishniac 1983): 3D high-resolution simulations have shown that such shells fragment into filaments and clumps (e.g. van Marle & Keppens 2012; Krause et al. 2013). The disturbed kinematics in the Krause (2005) simulations come from the strong early resistance of the unfragmented shell with high pressure build-up inside of it and strong gas acceleration when the shell eventually fragments due to other instabilities. If the shell in reality fragments earlier, the jet might even better pierce the immediate impact region between the clumps with less effect on the surrounding shell. This could be tested with dedicated simulations.

Alternatively, the spatial coincidence between jet and H I minimum could be purely a projection effect (in which case the H I minimum may be apparent due to the gas at this location being almost fully ionised), or that the jet punched through the gas sufficiently long ago that any turbulence has subsided (e.g. Krumholz et al. 2006). If we assume that the timescale for turbulent decay is similar to the crossing time of the emission-line region, back of the envelope calculations (dividing the size of the region by the assumed speed, adopting an initial turbulent velocity of 100 km s^{-1} , similar to velocities found e.g. from the simulation of Krause 2005 or the observations of Nesvadba et al. 2021, and a region size of 10 kpc) produce timescales of the order of 10^8 yr, which is comparable to the lower limit on the lobe age estimated in section 3.2. We would therefore expect any turbulent motions of this magnitude driven into the emission-line region by the expanding lobes not to be visible by the present time.

The picture that emerges from the assembled data is one with multiple events over different timescales. First, a tidal encounter left a $10^9 M_{\odot}$ cloud of H I around IC2497, and caused IC2497’s warped appearance. The new radio frequency data then show that a radio outburst, $\sim 10^8$ years ago, shaped and perturbed the multi-phase gas tens of kpc around IC2497, before switching off. The relic radio lobe from this outburst is what we now see in the LOFAR data – a corresponding northern radio lobe has presumably faded to invisibility, perhaps because of the lower gas density to the north of IC2497.

Much more recently ($\sim 10^5$ years ago) a radiatively-efficient AGN outburst illuminated the gas that had been swept up around the radio lobe and gave rise to the extended emission-line region that characterizes HV. The ongoing nuclear starburst and jet (both first observed by Rampadarath et al. 2010) may have begun/turned on around the same time but it seems unlikely that the jet was continuously active through the period. This timeline is clearly in contrast with the previous suggestion that fading AGN could indicate a lasting change in accretion mode (from being dominated by radiative to mechanical output; e.g. Sartori et al. 2018). In the IC2497-HV system, the situation is clearly more complex, with evidence for recurring episodes of mechanical (or radiatively inefficient) jet activity in addition to the radiatively efficient activity responsible for ionising HV.

We echo previous suggestions that HV could be a unique local object that exemplifies processes much more common in the high-redshift Universe at the peak of cosmic star formation, and is therefore worthy of more study.

ACKNOWLEDGEMENTS

DJBS dedicates this work to the loving memory of D.H.F. Smith (1943-2021): father, Chieftain, poet, and Voorwerp enthusiast. The authors would like to thank W.C. Keel for refereeing this paper, for providing the fully-processed *HST* tunable ramp filter data from Keel et al. (2012a), and for a preview of WIYN-HEXPAK observations of HV. We also thank G.I.G. Józsa for providing the FITS data products from Józsa et al. (2009). The authors would like to thank Paul Haskell and Soumyadeep Das for valuable comments. DJBS and MJH acknowledge support from the UK Science and Technology Facilities Council (STFC) under grant ST/V000624/1. LOFAR is the Low Frequency Array designed and constructed by ASTRON. It has observing, data processing, and data storage facilities in several countries, which are owned by various parties (each with their own funding sources), and that are collectively operated by the ILT foundation under a joint scientific policy. The ILT resources have benefited from the following recent major funding sources: CNRS-INSU, Observatoire de Paris and Université d'Orléans, France; BMBF, MIWF-NRW, MPG, Germany; Science Foundation Ireland (SFI), Department of Business, Enterprise and Innovation (DBEI), Ireland; NWO, The Netherlands; The Science and Technology Facilities Council, UK; Ministry of Science and Higher Education, Poland; The Istituto Nazionale di Astrofisica (INAF), Italy.

This research made use of the Dutch national e-infrastructure with support of the SURF Cooperative (e-infra 180169) and the LOFAR e-infra group. The Jülich LOFAR Long Term Archive and the German LOFAR network are both coordinated and operated by the Jülich Supercomputing Centre (JSC), and computing resources on the supercomputer JUWELS at JSC were provided by the Gauss Centre for Supercomputing e.V. (grant CHTB00) through the John von Neumann Institute for Computing (NIC).

This research made use of the University of Hertfordshire high-performance computing facility and the LOFAR-UK computing facility located at the University of Hertfordshire and supported by STFC [ST/V002414/1], and of the Italian LOFAR IT computing infrastructure supported and operated by INAF, and by the Physics Department of Turin University (under an agreement with Consorzio Interuniversitario per la Fisica Spaziale) at the C3S Supercomputing Centre, Italy.

DATA AVAILABILITY

The new LoTSS 150 MHz observations presented in this work are available from the LOFAR Surveys website, <https://www.lofar-surveys.org/> as part of the second data release of the LOFAR Two-metre Sky Survey (LoTSS).

REFERENCES

- Alexander D. M., Hickox R. C., 2012, *New Astron. Rev.*, **56**, 93
 Becker R. H., White R. L., Helfand D. J., 1995, *ApJ*, **450**, 559
 Biggs A. D., Younger J. D., Ivison R. J., 2010, *MNRAS*, **408**, 342
 Chabrier G., 2003, *PASP*, **115**, 763
 Condon J. J., Huang Z. P., Yin Q. F., Thuan T. X., 1991, *ApJ*, **378**, 65
 Condon J. J., Cotton W. D., Greisen E. W., Yin Q. F., Perley R. A., Taylor G. B., Broderick J. J., 1998, *AJ*, **115**, 1693
 Croton D. J., et al., 2006, *MNRAS*, **365**, 11
 Duncan K. J., et al., 2019, *A&A*, **622**, A3
 Duncan K. J., et al., 2021, *A&A*, **648**, A4
 Fabbiano G., Elvis M., 2019, *ApJ*, **884**, 163
 Gürkan G., et al., 2018, *MNRAS*, **475**, 3010
 Hardcastle M. J., Birkinshaw M., Worrall D. M., 1998, *MNRAS*, **294**, 615
 Harwood J. J., Hardcastle M. J., Croston J. H., Goodger J. L., 2013, *MNRAS*, **435**, 3353
 Heckman T. M., Best P. N., 2014, *ARA&A*, **52**, 589
 Hill G. J., et al., 2008, in Kodama T., Yamada T., Aoki K., eds, *Astronomical Society of the Pacific Conference Series Vol. 399, Panoramic Views of Galaxy Formation and Evolution*. p. 115 ([arXiv:0806.0183](https://arxiv.org/abs/0806.0183))
 Intema H. T., Jagannathan P., Mooley K. P., Frail D. A., 2017, *A&A*, **598**, A78
 Jaffe W. J., Perola G. C., 1973, *A&A*, **26**, 423
 Józsa G. I. G., et al., 2009, *A&A*, **500**, L33
 Kardashev N. S., 1962, *Soviet Ast.*, **6**, 317
 Keel W. C., et al., 2012a, *AJ*, **144**, 66
 Keel W. C., et al., 2012b, *MNRAS*, **420**, 878
 Keel W. C., et al., 2015, *AJ*, **149**, 155
 Kennicutt Robert C. J., 1998, *ARA&A*, **36**, 189
 Kondapally R., et al., 2021, *A&A*, **648**, A3
 Krause M., 2005, *A&A*, **431**, 45
 Krause M., Alexander P., 2007, *MNRAS*, **376**, 465
 Krause M., Fierlinger K., Diehl R., Burkert A., Voss R., Ziegler U., 2013, *A&A*, **550**, A49
 Krumholz M. R., Matzner C. D., McKee C. F., 2006, *ApJ*, **653**, 361
 Laing R. A., Peacock J. A., 1980, *MNRAS*, **190**, 903
 Lintott C. J., et al., 2008, *MNRAS*, **389**, 1179
 Lintott C. J., et al., 2009, *MNRAS*, **399**, 129
 Mao M. Y., et al., 2015, *MNRAS*, **446**, 4176
 Morabito L. K., et al., 2022, *A&A*, **658**, A1
 Morganti R., Garrett M. A., Chapman S., Baan W., Helou G., Soifer T., 2004, *A&A*, **424**, 371
 Moshir et al. M., 1990, *IRAS Faint Source Catalogue*, p. 0
 Nesvadba N. P. H., et al., 2021, *A&A*, **654**, A8
 Polletta M., et al., 2007, *ApJ*, **663**, 81
 Rampadarath H., et al., 2010, *A&A*, **517**, L8
 Rengelink R. B., Tang Y., de Bruyn A. G., Miley G. K., Bremer M. N., Roettgering H. J. A., Bremer M. A. R., 1997, *A&AS*, **124**, 259
 Sabater J., et al., 2019, *A&A*, **622**, A17
 Sabater J., et al., 2021, *A&A*, **648**, A2
 Sartori L. F., et al., 2018, *MNRAS*, **474**, 2444
 Schawinski K., et al., 2010, *ApJ*, **724**, L30
 Shimwell T. W., et al., 2017, *A&A*, **598**, A104
 Shimwell T. W., et al., 2019, *A&A*, **622**, A1
 Shimwell T. W., et al., 2022, *arXiv e-prints*, p. [arXiv:2202.11733](https://arxiv.org/abs/2202.11733)
 Shulevski A., et al., 2015, *A&A*, **583**, A89
 Silk J., Rees M. J., 1998, *A&A*, **331**, L1
 Singh V., Ishwara-Chandra C. H., Sievers J., Wadadekar Y., Hilton M., Beelen A., 2015, *MNRAS*, **454**, 1556

Smith D. J. B., et al., 2021, [A&A](#), 648, A6
Tasse C., et al., 2021, [A&A](#), 648, A1
Vishniac E. T., 1983, [ApJ](#), 274, 152
Williams W. L., et al., 2019, [A&A](#), 622, A2
York D. G., et al., 2000, [AJ](#), 120, 1579
de Gasperin F., et al., 2021, [A&A](#), 648, A104
van Haarlem M. P., et al., 2013, [A&A](#), 556, A2
van Marle A. J., Keppens R., 2012, [A&A](#), 547, A3
van Weeren R. J., et al., 2021, [A&A](#), 651, A115

This paper has been typeset from a $\text{\TeX}/\text{\LaTeX}$ file prepared by the author.